Spectrodirectional Minnaert-k retrieval using CHRIS-PROBA data

Verrelst, Jochem ; Schaepman, Michael E ; Clevers, Jan G P W

Abstract: We report on a detailed analysis of hyperspectral and multidirectional remote sensing data acquired using the Compact High Resolution Imaging Spectrometer (CHRIS) mounted onboard the Project for On-Board Autonomy (PROBA) spacecraft. This instrument is capable of sampling reflected radiation over the visible and near-infrared (NIR) region of the solar spectrum at a spatial resolution (approx. 17 m) intermediary between sensors traditionally used in land applications (such as Landsat and Satellite Pour l'Observation de la Terre (SPOT), 30 m–50 m) and the latest instruments delivering a nominal resolution of 1 m or less. The spectral anisotropic signature of an Alpine coniferous forest during winter in relation to canopy cover was investigated using the Minnaert-k parameter obtained by inverting the Rahman–Pinty–Verstraete (RPV) model against CHRIS data. Although earlier studies have demonstrated that Minnaert- k can be used to characterize surface heterogeneity at subpixel scale, its spectral dependency has not yet been fully assessed in an imaging spectrometry context. Minnaert-k parameter retrievals across CHRIS bands revealed that a switch from bell-shaped to bowl-shaped anisotropic reflectance patterns occurs when comparing visible to NIR responses. Specifically, the degree of canopy cover and background brightness determine where in the spectral domain this switch in reflectance anisotropy occurs. For a bright snow cover background Minnaert-k values correlated best with canopy cover at the end of the red edge (e.g., around 735 nm). In this spectral region, pixels with medium canopy cover (40%–70%) typically produced bell-shaped anisotropy patterns, while pixels with sparse (,30%) or dense (.70%) canopy covers typically produced bowl-shaped reflectance anisotropy patterns.

DOI: https://doi.org/10.5589/m11-012

Can. J. Remote Sensing, Vol. 36, No. 6, pp. 631–644, 2010

Spectrodirectional Minnaert-*k* retrieval using CHRIS-PROBA data

Jochem Verrelst, Michael E. Schaepman, Jan G.P.W. Clevers

Abstract. We report on a detailed analysis of hyperspectral and multidirectional remote sensing data acquired using the Compact High Resolution Imaging Spectrometer (CHRIS) mounted onboard the Project for On-Board Autonomy (PROBA) spacecraft. This instrument is capable of sampling reflected radiation over the visible and near-infrared (NIR) region of the solar spectrum at a spatial resolution (approx. 17 m) intermediary between sensors traditionally used in land applications (such as Landsat and Satellite Pour l'Observation de la Terre (SPOT), 30 m–50 m) and the latest instruments delivering a nominal resolution of 1 m or less. The spectral anisotropic signature of an Alpine coniferous forest during winter in relation to canopy cover was investigated using the Minnaert-*k* parameter obtained by inverting the Rahman–Pinty–Verstraete (RPV) model against CHRIS data. Although earlier studies have demonstrated that Minnaert-*k* can be used to characterize surface heterogeneity at subpixel scale, its spectral dependency has not yet been fully assessed in an imaging spectrometry context. Minnaert-*k* parameter retrievals across CHRIS bands revealed that a switch from bell-shaped to bowl-shaped anisotropic reflectance patterns occurs when comparing visible to NIR responses. Specifically, the degree of canopy cover and background brightness determine where in the spectral domain this switch in reflectance anisotropy occurs. For a bright snow cover background Minnaert-*k* values correlated best with canopy cover at the end of the red edge (e.g., around 735 nm). In this spectral region, pixels with medium canopy cover (40%–70%) typically produced bell-shaped anisotropy patterns, while pixels with sparse (<30%) or dense (>70%) canopy covers typically produced bowl-shaped reflectance anisotropy patterns.

Résumé. Nous rapportons une analyse détaillée de données hyperspectrales et multidirectionnelles acquises par le « Compact High Resolution Imaging Spectrometer » (CHRIS), monté sur la plateforme satellite « Project for On-Board Autonomy » (PROBA). Cet instrument est capable de mesurer la radiation réfléchie dans les régions visibles et proche infrarouge du spectre solaire à une résolution spatiale (~17 m) intermédiaire entre les capteurs traditionnellement utilisés pour les applications terrestres (tels que Landsat et Satellite Pour l'Observation de la Terre (SPOT) : 30 m–50 m) et les capteurs les plus récents qui offrent une résolution nominale 1 m ou moins. L'anisotropie spectrale de la signature d'une forêt conifère alpine en hiver en fonction du couvert de la canopée a été étudiée par l'intermédiaire du paramètre Minnaert-*k*, obtenu par inversion du modèle Rahman–Pinty–Verstraete (RPV) sur les données CHRIS. Bien que de précédentes études aient démontré que le paramètre Minnaert-*k* peut être utilisé pour caractériser l'hétérogénéité de la surface à l'intérieur d'un pixel, sa dépendance spectrale n'a pas encore été évaluée dans le contexte de l'imagerie hyperspectrale. Les valeurs du Minnaert-*k* obtenues pour les différentes bandes de CHRIS ont révélé que la courbe d'anisotropie de la réflectance passe de concave dans le visible à convexe dans le proche infrarouge. Spécifiquement, le degré de couvert de la canopée et de réflectance de l'arrière-plan détermine où le passage de concave à convexe a lieu dans le domaine spectral. Pour un arrière-plan de neige réfléchissante, les valeurs du Minnaert-*k* étaient le mieux corrélées avec le couvert de la canopée à la fin de la zone d'inflexion rouge (par exemple autour de 735 nm). Dans cette région spectrale, les pixels ayant un couvert moyen (40 %–70 %) ont typiquement produit des courbes d'anisotropie concaves, tandis que les pixels avec un couvert parsemé (< 30 %) ou dense (> 70 %) ont typiquement produit des courbes d'anisotropie convexes.

Introduction

The reflectance anisotropy of boreal and Alpine forests measured under winter conditions depends on the wavelength and the proportions and optical properties of the canopy and underlying snow cover that are recorded by a sensor (Nolin, 2004; Vikhamer and Solberg, 2003). These proportions depend on illumination and viewing angle, topography and structural canopy properties such as tree density and height, canopy geometry, and gap fraction. In the last 20 years, various studies have documented that anisotropic reflectance data encapsulate information about

Received 26 October 2010. Accepted 3 February 2011. Published on the Web at http://pubs.casi.ca/journal/cjrs on 8 July 2011.

Jochem Verrelst.[1] Department of Earth Physics and Thermodynamics, Image Processing Laboratory (IPL), Universitat de Valencia, P.O. Box 22085, E-46071 Paterna (Valencia), Spain; and Centre for Geo-Information, Wageningen University, Droevendaalsesteeg 3, 6708 PB Wageningen, The Netherlands.

Michael E. Schaepman. Remote Sensing Laboratories, University of Zurich, Winterthurerstrasse 190, CH – 8057 Zurich, Switzerland.

Jan G.P.W. Clevers. Centre for Geo-Information, Wageningen University, Droevendaalsesteeg 3, 6708 PB Wageningen, The Netherlands.

[1]Corresponding author (e-mail: jochem.verrelst@uv.es).

canopy structure at subpixel scale (e.g., Asner et al., 1998; Diner et al., 1999; Deering et al., 1999; Sandmeier and Deering, 1999). Yet, it was only with the development of surface reflectance models (e.g., Li and Strahler, 1992; Verhoef, 1984; Verstraete et al., 1990) and the advent of multiangular Earth-observing sensors (e.g., Barnsley et al., 2004; Diner et al., 1998) that significant progress was made in the retrieval of canopy characteristics from multiangular reflectance data (e.g., Canisius and Chen, 2007; Chopping et al., 2003; Diner et al., 2005; Gao et al., 2003; Pinty et al., 2002; Schaepman et al., 2005).

Among the surface reflectance models, the Rahman–Pinty–Verstraete (RPV) parametric model (Rahman et al., 1993) is particularly suitable for estimating reflectance anisotropy because it simulates the bidirectional reflectance distribution function (BRDF) of an arbitrary land surface on the basis of three (optionally four) parameters. Of these parameters, the k parameter is of particular interest as it can be related to canopy structure provided there is sufficient contrast between the darker overstory and brighter background at that wavelength (Pinty et al., 2002; Widlowski et al., 2001, 2004).

Several studies have mapped Minnaert-k as a proxy for vegetation structure and density at the subpixel scale for various landscapes such as prairie, woodland, and forest (Lavergne et al., 2007; Nolin, 2004; Pinty et al., 2002; Sedano et al., 2008). All these studies used Multi-angle Imaging SpectroRadiometer (MISR) satellite data or its airborne variant AirMISR. MISR, on board the National Aeronautics and Space Administration (NASA) Terra platform, is configured with nine cameras, each observing the Earth in four spectral bands. In the global data acquisition mode, eight oblique cameras observe the Earth's surface at a resolution of 1100 m in blue, green, and near-infrared (NIR) bands and at a resolution of 275 m in the red domain. In addition, all four bands of the nadir-observing camera have a spatial resolution of 275 m (Diner et al., 1998). Pinty et al. (2002) reported that the availability of sufficient brightness contrast between overstory and background in conjunction with a relatively high sun position (sun zenith $<60^{\circ}$) is instrumental to correctly exploit the Minnaert-k parameter in the interpretation of the anisotropy of the reflectance. They also demonstrated that the potential to detect canopy structural information from multiangular measurements depends on the sensor's spatial resolution. Typically, the higher the spatial resolution the more opportunities exist to detect reflectance anisotropy at the corresponding subpixel scale.

In 2001, 2 years after the launch of Terra, the European Space Agency (ESA) launched the experimental satellite sensor Compact High Resolution Imaging Spectrometer (CHRIS) onboard the Project for On-board Autonomy (PROBA) spacecraft. The pushbroom imaging spectrometer is the first high spatial resolution sensor with advanced pointing capability dedicated to the acquisition of nearly simultaneous images with multiple view angles. CHRIS acquires a series of five images of a terrestrial surface at a high spatial resolution (up to approx. 17 m) during the same overpass. Depending on its operating mode, CHRIS is capable of sampling the anisotropic behaviour of the reflected solar radiation in up to 62 narrow spectral bands covering the visible and NIR (VNIR) region of the solar spectrum. The high spatial resolution of CHRIS is of specific interest to study reflectance anisotropy at the forest stand scale.

A set of concurrent multiangular CHRIS images of an old-growth alpine forest stand (see "Test site") was acquired during winter to characterize the structural properties of the observed forest using the Minnaert-k parameter. Because the spatial resolution of CHRIS (approx. 17 m) is of the same order of magnitude as the typical dimension of trees in our field site (approx. 12 m), we now have an opportunity to investigate the canopy structure of such a stand in great detail. Though Koetz et al. (2005) have demonstrated that the k parameter can be partially related to structural parameters at the CHRIS subpixel scale, the spectral dependency of these relationships has not yet received full attention. We therefore formulated two research objectives: (*i*) to evaluate the spectral dependency of the Minnaert-k parameter retrieved from coniferous stands during winter over the VNIR spectral range and (*ii*) to interpret the parameter's underlying wavelength-dependent biophysical meaning. Both objectives were intended to elucidate the anisotropic reflectance properties of forested surfaces recorded with a high spatial resolution sensor like CHRIS. This improved understanding can serve as a benchmark for interpreting spectrodirectional (combined spectral and multiangular) data and may trigger new methods that exploit the angular domain in a more physically-based way.

Biophysical interpretation of Minnaert-*k*

The RPV model provides a phenomenological description of the target's anisotropy without attempting to assign it to specific physical causes or processes. As such, it is an empirical and efficient parametric representation of that surface property. The RPV model splits the BRF field for a given wavelength (λ) into a scalar amplitude component (ρ_0) and an associated directional component describing the anisotropy of the surface (Rahman et al., 1993; Pinty et al. 2002). The directional component is expressed as the product of three functions, each dependent on a single parameter: (*i*) the modified Minnaert function (k) that controls the curvature of the scattering regime, (*ii*) the Henyey–Greenstein function (Θ) that controls the degree of forward and backward scattering regimes, and (*iii*) a hotspot descriptor function (ρ_c). The dependency of these functions on their respective parameters is documented in the abovementioned publications. The empirical parameter, k, of the Minnaert's function (Minnaert, 1941) is particularly interesting because it quantifies the extent to which the angular variations in the BRF pattern resemble a

"bell-shaped" or "bowl-shaped" pattern (Pinty et al., 2002). It has been proven that under favourable illumination conditions and a large brightness contrast between a relatively light background (e.g., soil or snow) and relatively dark vertical structures (e.g., trees) the angular pattern is largely controlled by the physical properties and geometric arrangements of the plant elements (Pinty et al., 2002; Widlowski et al., 2001). Hence, an analysis of the angular signature in a specific spectral band can provide structural information on the target at a subpixel spatial scale provided there is sufficient contrast between the darker overstory and brighter background in that band.

Coniferous forests commonly appear darker in the visible region than deciduous forests because of the strong internal shadowing caused by clumping effects and the relatively high light absorption capacity of needles (Smolander and Stenberg, 2003). Open canopies composed of tall trees in conjunction with a bright snow background means that boreal or alpine winter landscapes offer ideal conditions for Minnaert-k analysis. Given a sufficiently low solar zenith angle (i.e., $<60^{\circ}$; Pinty et al., 2002), the following situations can occur in coniferous stands during winter:

(i) Surfaces that are brighter at large oblique viewing angles in forward and backward scattering directions lead to a bowl-shaped reflectance anisotropy pattern. Enhanced scattering towards larger zenith angles typically occurs in cases of closed and structurally homogeneous forests or in cases of single-layer surfaces, such as bare soil or snow cover. Bowl-shaped anisotropy patterns result in k values <1.

(ii) Conversely, surfaces that are brighter at the nadir viewing angle than at oblique viewing angles lead to the inverse pattern: a bell-shaped reflectance anisotropy pattern. In open, vertically elongated canopies, the contribution of uncollided radiation to the total signal (i.e., the fraction of radiation that has travelled through the gaps of the canopy layer and has been scattered by the background only (Pinty et al., 2004)) is maximized at the nadir viewing angle while at greater zenith angles it is intercepted by the tall trees. Bell-shaped anisotropy patterns result in k values >1.

(iii) Surfaces that exhibit lambertian reflectance (i.e., the amount of scattered radiation is the same in all directions) result in a k value of 1.

The Minnaert-k value can thus essentially be used as a proxy for canopy heterogeneity simply on the basis of canopy closure and fluctuations in the amount of scattering and absorbing material at one specific wavelength. It has been successfully used to characterize the structural heterogeneity of canopies over snow (Nolin, 2004). We explore how this relation between the Minnaert-k parameter and canopy structure changes with wavelength within the VNIR spectral domain.

Test site

The chosen test site is located in an Alpine valley, the Ofenpass, in the Swiss National Park in the Engadine region, southeast Switzerland (10°13′48″E, 46°39′45″N). The Ofenpass represents a dry inneralpine valley with limited precipitation (900–1100 mm/year) at an average altitude of about 1900 m above the mean sea level. Two subalpine ecosystems, a coniferous old-growth forest and a meadow, cover the south-facing slope. The forest is dominated by mountain pine (*Pinus Montana* subsp. *arborea*) and some stone pine (*Pinus cembra*) tree species. These forest stands can be classified as woodland associations of the *Erico-Pinetum mugo* type, typified by relatively open discontinuous stands. The forests vary in topography, openness, tree clumping, leaf area index (LAI), and woodiness (Kötz et al., 2004; Verrelst et al., 2008). Typical tree height is 11.9 ± 2.9 m. The south-facing valley floor of the Ofenpass valley was considered to be the core test site (see box in **Figure 1**). Stand variables of the core test site are provided in **Table 1**.

CHRIS data

PROBA is an experimental ESA platform that enables CHRIS to capture near-concurrent multiple views of a surface in a short period of time. CHRIS uses the satellite's tilting and pointing capabilities in along-track and across-track directions allowing the acquisition of up to five images during a few minutes (Barnsley et al., 2004). CHRIS can be operated in five different modes, with different combinations of band configuration (number, centre location, and width) and spatial resolution for specific applications (e.g., aerosols, land, or water).

A set of CHRIS mode 5 land images were acquired over the Swiss National Park site on 17 March 2007 near noon

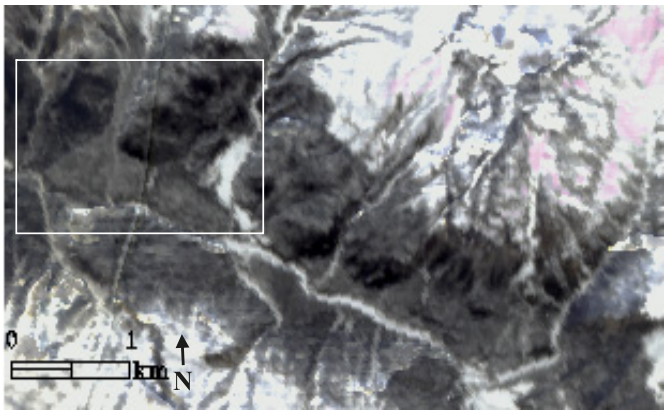

Figure 1. Red–green–blue (RGB) subset of the geometrically and atmospherically corrected CHRIS-PROBA nadir scene acquired over the Swiss National Park study site on 17 March 2007. The Ofenpass valley stretches from upper left to bottom right of the image. The core test site is boxed. The white part within the box is the snow-covered meadow. (R,631 nm, G 550 nm, B 442 nm.)

Table 1. Stand variables for the core Ofenpass test site (south-facing valley floor).

Variable	Generic field observations
Stand structure	
Stand age (years)	165–200
Tree height (m)	11.9 ± 2.9
Crown radius (m)	0.9
Crown base (m)	7.0
Stand density (trees/ha)	790 ± 250 (>12 cm DBH)
Within-crown structure	
Crown LAI ($m^2/m^{2)}$	1.5–4.5
Crown photosynthetic vegetation (%)	60–90

Note: Data were collected during the SPREAD field campaign (Kötz et al., 2004; Morsdorf et al., 2004).

(1134) local time under cloud-free conditions. Mode 5 is configured in CHRIS's best spatial resolution (nominally approx. 17 m) and spectral resolution (37 narrow spectral bands with bandwidths of 6–33 nm located between 438 nm and 1036 nm). Its specifications are summarized in **Table 2**. The large number of spectral bands enables, among other things, the anisotropic spectral behaviour to be examined in the transition zone between the visible and NIR, the "red edge", as there are eight CHRIS bands in the spectral domain ranging from 700 nm to 750 nm. Several monoangular nadir studies have shown that measurements based on the red edge position correlated well with biophysical variables such as LAI (e.g., Clevers et al., 2002) at canopy scale. However, only scant attention has been paid to the directional domain of the red edge (i.e., how the curvature of the anisotropic reflectance responds to canopy structure).

The acquisition date was chosen to ensure that a snow carpet was still present while the sun position was already acceptably high at noon (sun zenith 50°, azimuth 161°; see polar plot of **Figure 2**). The solar position can be regarded as constant for all five CHRIS fly-by zenith angles; the time elapsed between the first and last recordings during the satellite overpass was less than two minutes. In the current along-track pointing configuration, the fly-by zenith angles are equivalent to the nominal viewing zenith angles (VZA: nadir, $\pm 36°$, $\pm 55°$). However, because CHRIS has a narrow field of view (FOV), CHRIS is only occasionally able to acquire a target at nominal view angle. PROBA must be tilted so that the target area falls within the sensor's FOV (Barnsley et al., 2004). This means that the actual observation angles at which the images are acquired may deviate from the nominal view angles. For example, the nominal nadir camera position happened to be pointed in a forward VZA of +21°.

The exact viewing geometries of all five CHRIS view angles and the sun position are shown in the polar plot of **Figure 2**. A subset of the near-nadir image of the Ofenpass valley overpass is depicted in **Figure 1**. The dark parts in the figure are the forest vegetation; the white patch within the dark forest represents a snow-covered meadow. Note that snow quality also influences the shape of the reflectance anisotropy patterns (Painter and Dozier, 2004; Warren et al., 1998). From snow and weather information provided by the Swiss Federal Institute for Snow and Avalanche Research (SLF) we know there was no snowfall that week in the Engadine region (14–17 March 2007: no snowfall, cloud-free). This was also noted during a field visit to the region during the PROBA overflight. Snow on the branches of the trees had melted, which means that the "snow-covered forest" had snow on the ground, but not on the trees. Following a comparison of CHRIS spectral signatures with those of the John Hopkins spectral library (Salisbury et al., 1994) the snow grain size diameter was assessed as medium. Hardly any spatial variation in snow grain size was noted, which suggests that the influence of snow grain size on reflectance anisotropy at the pixel scale can be considered as negligible.

Methods of data analysis

The CHRIS scenes acquired at various angles were corrected to account for the topographic effect of rugged, mountainous terrain, following the approach developed by Kneubühler et al. (2005). A parametric approach for geometric correction of each CHRIS acquisition (up to five viewing angles) was applied; it was based on a 3D physical model (Toutin, 2004). The data from the angular observations were resampled to a common grid of 18 m. This method allowed us to achieve high geometric accuracy with a geolocation uncertainty of about half a pixel across and along track when using a digital terrain model (DTM; Swisstopo, Wabern, Switzerland) with 2 m resolution. Regrettably, the backward-pointing $-55°$ view zenith angle just missed the test site. The remaining four images were atmospherically corrected using a freely available moderate resolution atmospheric transmission (MODTRAN) based atmospheric correction module (Guanter et al., 2005) implemented in the Basic ERS and Envisat (A)ATSR and Meris Toolbox (BEAM) Toolbox (http://www.brockmann-consult.de/beam) that has been specifically developed for correcting CHRIS images. The method is designed to automatically derive aerosol loading, columnar water vapor, and surface reflectance from CHRIS data as well as to update CHRIS's spectral and radiometric calibration parameters when necessary (Guanter

Table 2. Compact High Resolution Imaging Spectrometer (CHRIS) specifications for Land Mode 5.

Sampling	Image area	View angles	Spectral bands	Spectral range
~17 m at 556 km altitude	13 km × 13 km (766 × 748 pixels)	5 nominal angles at −55°, −36°, 0°, +36°, +55°	37 bands of 6–33 nm width	438–1036 nm

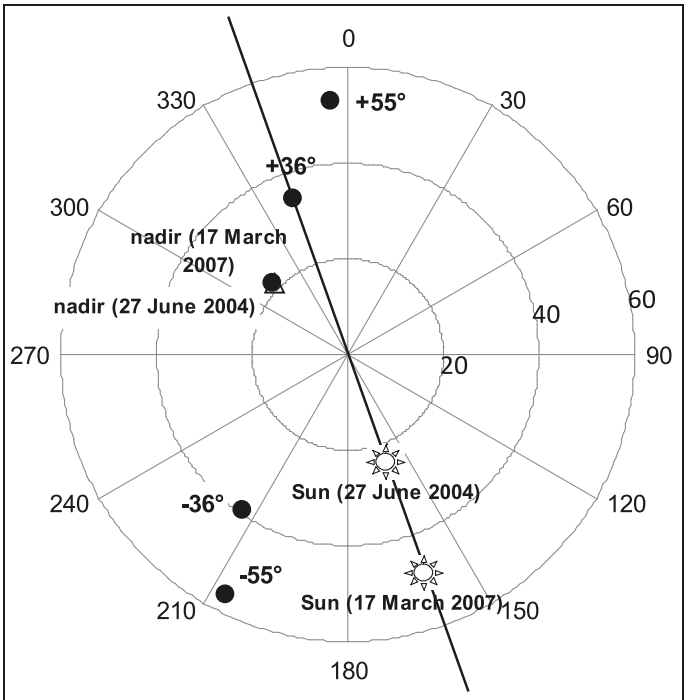

Figure 2. Polar plot of illumination geometry (sun symbol) and CHRISimage acquisition as of 17 March 2007 (solid circle), and nadir acquisition geometry as of 27 June 2004 (open triangle). The nominal −55° view zenith angle missed the test site. (PP, principal plane.)

et al., 2005). The preprocessing efforts resulted in geometrically corrected images of hemispherical-directional-reflectance-factor (HDRF) data (Schaepman-Strub et al., 2006). The observations at 442 nm and 489 nm were removed from the analysis because of significant atmospheric scattering in the blue bands of CHRIS. Moreover, bands close to the atmospheric water vapor absorption band at 940 nm (CHRIS bands at 925 nm, 940 nm and 955 nm) were also omitted from further analysis. For all remaining 32 bands the Minnaert-*k* parameter was calculated.

Minnaert-*k* retrieval

For each pixel, the Minnaert-*k* parameter was retrieved by inverting the RPV model using the three-parameter RPV inversion software package (Lavergne et al., 2007). The package offers a number of features, including the complete assessment of the measurement-model mismatch covariance matrix and the option of operating adjoint software codes derived from automatic differentiation techniques. This allowed us to perform the inversion of the nonlinear RPV model under the classical Bayesian approach in a numerically and computationally efficient manner, while at the same time generating an unbiased estimation of the probability density functions (PDFs) for the parameters retrieved. The package implements the inverse model for two versions of the model: the standard version using three parameters and an extra version with the hot spot parameter in addition. The hotspot parameter is only required to improve the representation of the hotspot when illumination and observation geometries close to the hotspot are present. In the observed winter scene of CHRIS, this configuration was not of importance. The RPV inversion-3 procedure thus resulted in sets of RPV parameters (ρ_0, k, and Θ) and additional information on the accuracy of the fit expressed by the χ^2 value. Measured and modeled data were compared using the χ^2 test (for a significance level $\alpha = 0.05$) to evaluate the performance and the fit of the model parameters. More detailed information about the applied inversion procedure can be found in Lavergne et al. (2007).

Reference map

Simultaneous exploitation of the spectral and directional behaviour of vegetation canopies allows canopy biophysical and biochemical properties to be assessed on the basis of variations in the reflectance signatures, and at the same time, provides additional information on canopy structure on the basis of variations in the angular signatures. Regarding the latter, the aim of this study was to identify how they change across the spectral domain and to identify the spectral region where reflectance anisotropy is most closely related to canopy structure. To do so, it is of interest to select the structural parameter that most affects the reflectance anisotropy so that the resulting map can be used as a reference for evaluating the Minnaert-*k* parameter across the spectral domain. Widlowski et al. (2001) and Pinty et al. (2002) have already reported the importance of the background contribution. Kayitakire and Defourny (2004) concluded that in forested landscapes the horizontal arrangement of the trees and the stand density influence the anisotropy of the canopy reflectance more than tree height and diameter. Koetz et al. (2005) used LiDAR data to try establishing a relationship between the Minnaert-*k* parameter and canopy cover and tree height, but that approach does not provide information about the background brightness. To assess the relationships of the Minnaert-*k* parameter with structural information across the CHRIS wavelengths, it therefore seems more logical to use a canopy cover map that is spectrally derived. Because illuminated snow and coniferous tree crowns are spectrally highly distinct (Vikhamar and Solberg, 2003), a canopy cover map was generated from the near-nadir CHRIS image by applying linear spectral unmixing (LSU). LSU is a technique commonly applied to derive canopy cover maps from hyperspectral data (Chen et al., 2004; Sabol et al., 2002). Canopy cover is defined as the percentage (from 0% to 100%) of a grid cell that is covered by plant canopy when imaged from above. LSU analysis was developed to decompose image pixels into their pure constituents (Adams et al., 1995; Settle and Drake, 1993), which under winter conditions means vegetation and snow cover. LSU assumes that the reflectance at pixel scale can be described by a spectral mixture model in which a mixed spectrum is represented as a

linear combination of spectral endmembers (Equation (1))

$$R_i = f_{\text{vegetation}} \cdot R_{i,\text{vegetation}} + f_{\text{snow}} \cdot R_{i,\text{snow}} + \varepsilon_i \quad (1)$$

under constraint

$$f_{\text{vegetation}} + f_{\text{snow}} = 1 \qquad \text{and } f > 0 \quad (2)$$

where $f_{\text{vegetation}}$ and f_{snow} are the fractions of vegetation and snow in the pixel studied, R_i is the reflectance of a pixel in band i, $R_{i,\text{ vegetation}}$ ($R_{i,\text{ snow}}$) is the reflectance of the vegetation (snow) endmember in band i, and ε_i is the residual error associated with band i. The unmixing was forced to be fully constrained (Equation (2)). This guaranteed a physical interpretation of the results, because the fractions sum to 1 and all the fractions are positive (Zurita-Milla et al., 2007). The fit of the model can be assessed by the root mean square error (RMSE):

$$\text{RMSE} = \sqrt{\frac{\sum_{b=1}^{i} \varepsilon_b{}^2}{i}} \quad (3)$$

where i is the number of bands used in the spectral unmixing. The full spectral domain (excluding the bands we had removed) was used to unmix the near-nadir image into these two endmembers. The endmembers are depicted in **Figure 3**. The snow endmember was extracted from 16 fully snow-covered central meadow pixels of the near-nadir CHRIS data. Hardly any spectral variation was noted. The vegetation endmember was extracted from 94 dense, fully vegetated forest cover pixels of the core test site using summer near-nadir CHRIS data (27 June 2004; see Verrelst et al. (2008) for more information) to avoid contamination from snow cover underneath the canopy layer. As during summer, the forest is characterized by a vegetated understory (rejuvenates, shrubs), and more spectral variation was noted. Hence, the averaged spectral variation resembles a generic, photosynthetically active vegetation signature. The CHRIS near-nadir viewing geometry of the summer acquisition (open triangle) precisely matched the CHRIS near-nadir viewing geometry of the winter acquisition (solid circle) (**Figure 2**). We know of no events (e.g., storms) that may have significantly altered the forest structure in the last few years. While recognizing the limitations of applying LSU at high spatial resolution data because of multiple scattering from the targets (Borel and Gerstl, 1994), the advantage lies in the technique's compatibility with the used data set. The unmixing quantified the subpixel spectral contributions of overstory canopy cover and underlying snow cover proportions on the basis of the spectral dimension of monoangular, near-nadir CHRIS measurements thereby minimizing uncertainties related to geolocation and spatial resampling. The unmixing approach for the forest site was tested pixelwise on its uncertainty as expressed by the RMSE. As there were only two endmembers, the RMSE values were consistently low (around 0.016). The results were compared with ground reference data collected for four plots (20 m × 20 m) according to the Validation of Land European Remote Sensing Instruments (VALERI) protocol during the Fire Spread and Mitigation (SPREAD) campaign (Kötz et al. 2004; Morsdorf et al., 2004). Consistent results were obtained, with a slight overestimation of canopy cover of about 8% when compared with the ground reference data.

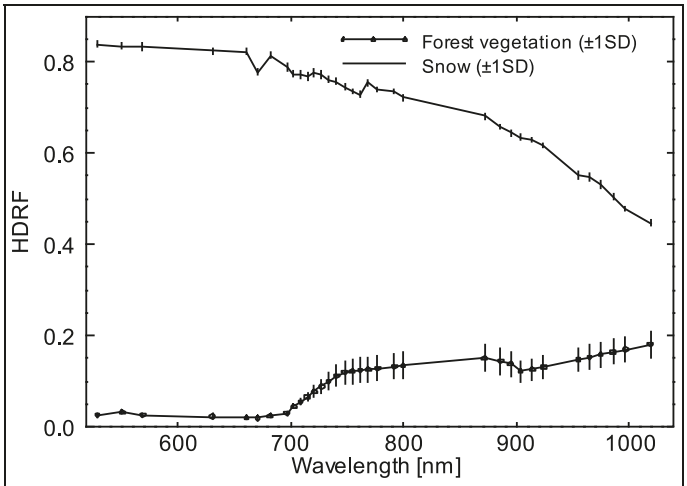

Figure 3. Snow and forest vegetation endmembers extracted from near-nadir images (average and standard deviation). The small spikes in the snow endmember are artifacts of the atmospheric correction (L. Guanter, personal communication, 2009).

Results

Spectral maps of the Minnaert-*k* parameter

Minnaert-*k* maps of the core test site were generated on a pixel-by-pixel basis across all of the used CHRIS wavelengths. The wavelengths ranged from the green (530 nm) to the NIR (1019 nm). Six of these maps are shown in **Figure 4**. The accuracy of the retrieval for each pixel was calculated using the χ^2 test. Despite the limited number of angular observations, the RPV model was able to fit the CHRIS angular signatures for the Ofenpass valley with high accuracy for most of the pixels. The best χ^2 results were for the forest vegetation on the valley floor. Misfits at the 5% significance level typically occurred along the forest edges, riverbeds, steep slopes, and in some bands over snow-covered regions. In particular, the sudden change in volumetric structure on the forest–meadow interface led to unexpected shapes of anisotropy. All pixels with a misfit were filtered out in further analysis. Considering the Minnaert-*k* retrievals, systematic and pronounced anisotropy patterns emerged in both the spatial and spectral dimensions. The series of Minnaert-*k* maps show that anisotropy patterns shift from predominantly bell-shaped patterns ($k > 1.0$; in blue colour tones) at the shorter wavelengths towards predominantly bowl-shaped patterns ($k < 1.0$; in red colour tones) at the longer wavelengths. These maps also suggest that the largest variability of bell- and bowl-shaped patterns

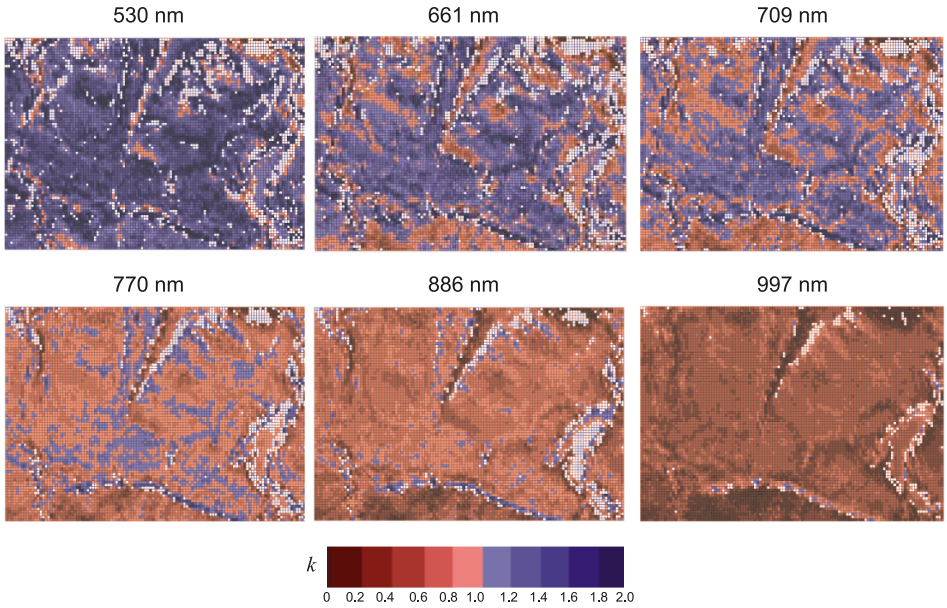

Figure 4. Minnaert-*k* maps for various CHRIS wavelengths. The white pixels are those in which the reflectance anisotropy of the CHRIS–HDRF data and the RPV-reconstructed HDRF data was significantly different.

is located around the red edge region. A more systematic overview of the Minnaert-*k* dynamics across the full spectral range of CHRIS is provided in **Figure 5**. The figure shows the spectral dependency of the *k* values averaged for the core study site in conjunction with their standard deviations. The progressively decreasing trend underlines the strong spectral dependency of the Minnaert-*k* parameter. In the visible region, bell-shaped reflectance anisotropy patterns dominate ($k > 1.0$); the bright background controls the reflectance of the entire scene at smaller zenith angles (e.g., near-nadir) while at larger zenith angles the absorbing properties of the coniferous trees control the reflectance. Conversely, in the NIR spectral region bowl-shaped reflectance anisotropy patterns dominate ($k < 1.0$) because of enhanced transmission and multiple scattering processes of NIR radiation throughout the canopy (Sandmeier and Deering, 1999). As a consequence of these multiple scattering processes, the brightness contrast between canopy components and background diminishes, particularly further into the NIR. This leads to lower *k* values that vary within a limited numerical range in the NIR which hampers the separation of different canopy structures, although some spatially distinct features remain visible. For instance, up to the 886 nm map, the riverbed (centre, below) and the edges of the homogeneous snow-covered meadow exhibit a pronounced bell-shape while at the 997 nm map the spatial patterns remain visible, but *k* values hardly reach 1. The spatial patterns of contrasting low and high *k* values can be explained by extreme topographic features (i.e., by slope and aspect effects, or by subpixel landscape features with extreme spectral contrast, such as roads or riverbeds transecting the area of vertically elongated coniferous trees).

Biophysical interpretation Minnaert-*k* maps

As it became evident that the Minnaert-*k* parameter is influenced by wavelength, our next step was to analyze the parameter's underlying physical meaning. For this analysis we used CHRIS data of the forest on the south-facing valley floor. Although most of the erratic, mountainous terrain was excluded from the analysis, subtle variations in topography may still lead to target occlusions or larger degrees of anisotropy and thus affect the inversion results. Further interpretations of the retrieved model parameters were therefore restricted to forested areas on south-facing slopes with a maximum steepness of 7°. In an earlier study, tests on the influence of topographic variables using multiple regressions revealed that this approach would sufficiently decouple the topographic effects (Verrelst et al., 2008). We are therefore justified in assuming that remaining surface anisotropy is controlled predominantly by canopy structure and density.

Because the curvature of the angular signature strongly depends on the relative proportion of scattering from the overstory and the background, the independently derived canopy cover map was used as a base map for the biophysical evaluation. The canopy cover map was stratified into seven canopy cover classes starting with 20% and with subsequent increments of 10% up to 90% cover. Canopy cover classes lower than 40% are referred to as "sparse", canopy cover classes above 70% are referred to as "dense" and all the intervening canopy cover classes are referred to as "medium dense". The abrupt transition from flat, homogeneous land cover types to more volumetric land cover types is known to significantly impact the horizontal radiation fluxes (e.g., Widlowski et al., 2006). No pixels in the 0%–20% canopy

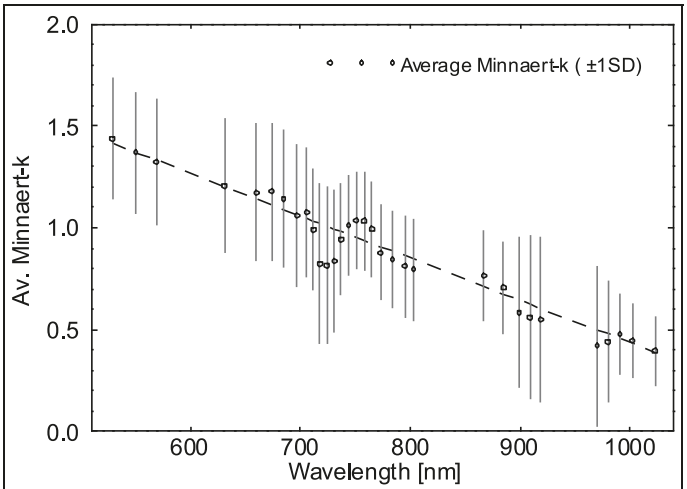

Figure 5. Average Minnaert-*k* and standard deviation (SD) as a function of wavelength. A linear trend line has been added.

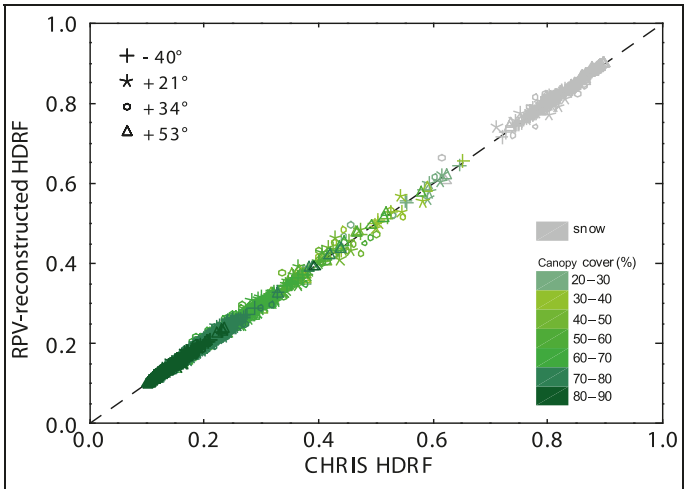

Figure 6. Comparison of CHRIS–HDRF and RPV-reconstructed HDRF at 631 nm for various canopy cover classes.

cover class were included, as most of them occurred along meadow and river edges. Hence, only pixels within the continuous forest were used for further analysis. As an example, the performance of the RPV inversion for these canopy cover classes and the snow-covered meadow using the four viewing angles at 631 nm is shown in **Figure 6**. This figure shows the relationship between the measured CHRIS–HDRF data, the RPV-reconstructed HDRF data, and the canopy cover classes and pure snow pixels taken from the snow-covered meadow field. For the majority of the angular measurements a one-to-one relation was found, which emphasizes the good performance of the inversion. The angular measurements that deviated from the one-to-one line tended to be the mid-angular measurements (near-nadir and +34° VZA). This is because not all pixels showed an unambiguous bell or bowl shape, but instead tended to show an irregular curvature for which the RPV-reconstructed HDRF values optimized a smoother curvature in between the irregular curvature.

Using canopy cover as a spatial mask, the averaged Minnaert-*k* value was calculated for each wavelength and canopy cover class (**Figure 7**). The figure shows a systematic, gridded overview of Minnaert-*k* values plotted for the wavelengths recorded by CHRIS along the *x*-axis and the canopy cover along the *y*-axis. Each grid cell represents the averaged Minnaert-*k* value for a specific cover class and wavelength. For a few grid cells the associated averaged angular signature is illustrated. The column of numbers immediately to the right of the central panel shows the number of pixels in each canopy cover class. Note that 94% of the pixels have a canopy cover of 60% or more. Only very few pixels with low canopy cover (<40%) are available, potentially weakening the robustness of the results in this range; nevertheless, the dynamics detected are sufficiently comprehensive in this figure.

Figure 7 illustrates how the anisotropic spectral behaviour is controlled by the interactions between canopy cover and wavelength. The underlying radiative transfer dynamics that control the variations of the gridded Minnaert-*k* results are further explained with the help of the example figures illustrated in the four panels of **Figure 8**. These figures display the spectral trajectories of the averaged anisotropic reflectance signatures for sparse (a, 20%–30%), medium dense (b, 40%–50%; c, 50%–60%; and d, 60%–70%), and dense (e, 70%–80%; and f, 80%–90%) canopy cover classes. As can be observed from **Figures 7** and **8**, canopy cover essentially determines the importance of vegetated overstory and snow cover relative to the total top of canopy reflectance and determines the curvature of the angular signature. For example, it controls whether stand HDRF values peak at near-nadir zenith angles (e.g., in case of open canopies) or at higher zenith angles (e.g., in case of closed canopies). Not only the canopy density but also the wavelength controls the curvature of the angular signature, and thus the value of the *k* parameter. This will be demonstrated in the next section.

For almost all canopy cover classes, the signatures at shorter wavelengths are characterized by bell-shaped patterns. Only the sparse canopy cover (**Figure 8a**, 20%–30%) gave rise to bowl-shaped anisotropy patterns. The absorptive properties of the sparse tree cover did not exert sufficient influence to alter the surface-leaving bowl-shaped reflectance field into a bell-shaped field. Instead, this bowl-shape remained unchanged throughout the spectral domain. The uncollided forward scattering of snow cover and, from the red edge onward, some contribution of multiple scattering due to sparse tree cover led solely to enhanced HDRF values at greater zenith angles. Because of the low number of pixels this class should nevertheless be interpreted with care.

When there is a denser canopy cover, the contribution of uncollided radiation scattered from the bright snow background to the total reflectance is greatest at near-nadir viewing angles and decreases at larger zenith angles as it becomes obscured by the vertical trees and therefore results in a bell-shaped reflectance

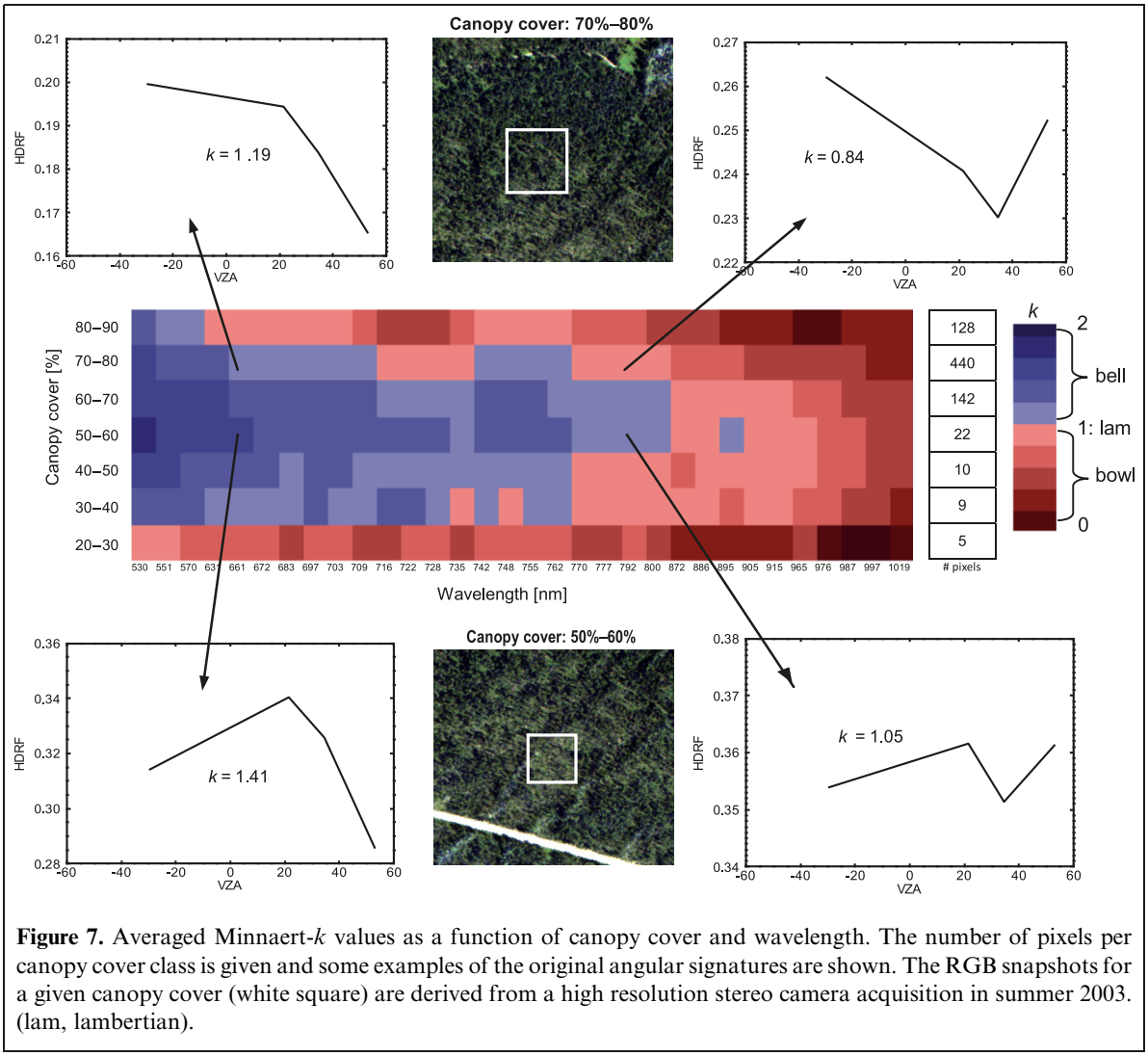

Figure 7. Averaged Minnaert-*k* values as a function of canopy cover and wavelength. The number of pixels per canopy cover class is given and some examples of the original angular signatures are shown. The RGB snapshots for a given canopy cover (white square) are derived from a high resolution stereo camera acquisition in summer 2003. (lam, lambertian).

pattern. Subsequently, when the red edge region is entered, a combination of two independent processes at subpixel level affects the top-of-canopy reflectance anisotropy: (*i*) an ongoing decrease of scattered radiation that exits the snow background due to increased absorption by snow grains and particularly (*ii*) an increase in multiple scattering processes that govern the dispersion processes of radiation exiting throughout the canopy. Both processes tend to reduce the bell-shaped pattern; a more absorbing background starts to mimic the reflectance pattern of vegetation, and a high scattering of the foliage will enhance the bowl-shaped pattern. In addition, the degree of canopy openness and background brightness will determine where in the spectral domain a bell-shaped pattern will turn into a bowl-shaped pattern. These processes are clearly illustrated for canopy covers ranging between 40% and 50% (**Figure 8b**) and 70% and 80% (**Figure 8e**). Bell-shaped anisotropy signatures are prominently present in the visible spectral region of both cover classes and even enter the red edge. At a certain wavelength, however, the snow reflectance is no longer able to provide maximum values at smaller zenith angles. Induced by the enhanced multiple scattering processes throughout the canopy and which start to be important from the red edge onward, high reflectance values at larger zenith angles become dominant; a transition into a bowl shape takes place. This transition will occur more quickly with greater tree cover, as the influence of uncollided radiation from the bright snow background is then diminished while the multiple scattering effects are further enhanced. At medium dense canopy covers (40%–70%), a bell shape holds until the early NIR (803 nm); thereafter, enhanced scattering at larger zenith angles starts to lead to a bowl shape. At denser canopy cover (70%–80%), the shift from a bell shape to a bowl shape happens more rapidly (i.e., at the beginning of the red edge (716 nm)).

At even denser canopy cover (between 80% and 90%, **Figure 8f**), the tree crowns are so densely packed that there is hardly sufficient uncollided radiation exiting the snow background available to produce a bell-shaped pattern. Once the red edge is reached, the predominantly multiple scattering processes throughout the canopy immediately outperform the influence of single scattering from the snow layer and cause a shift to a bowl-shaped pattern.

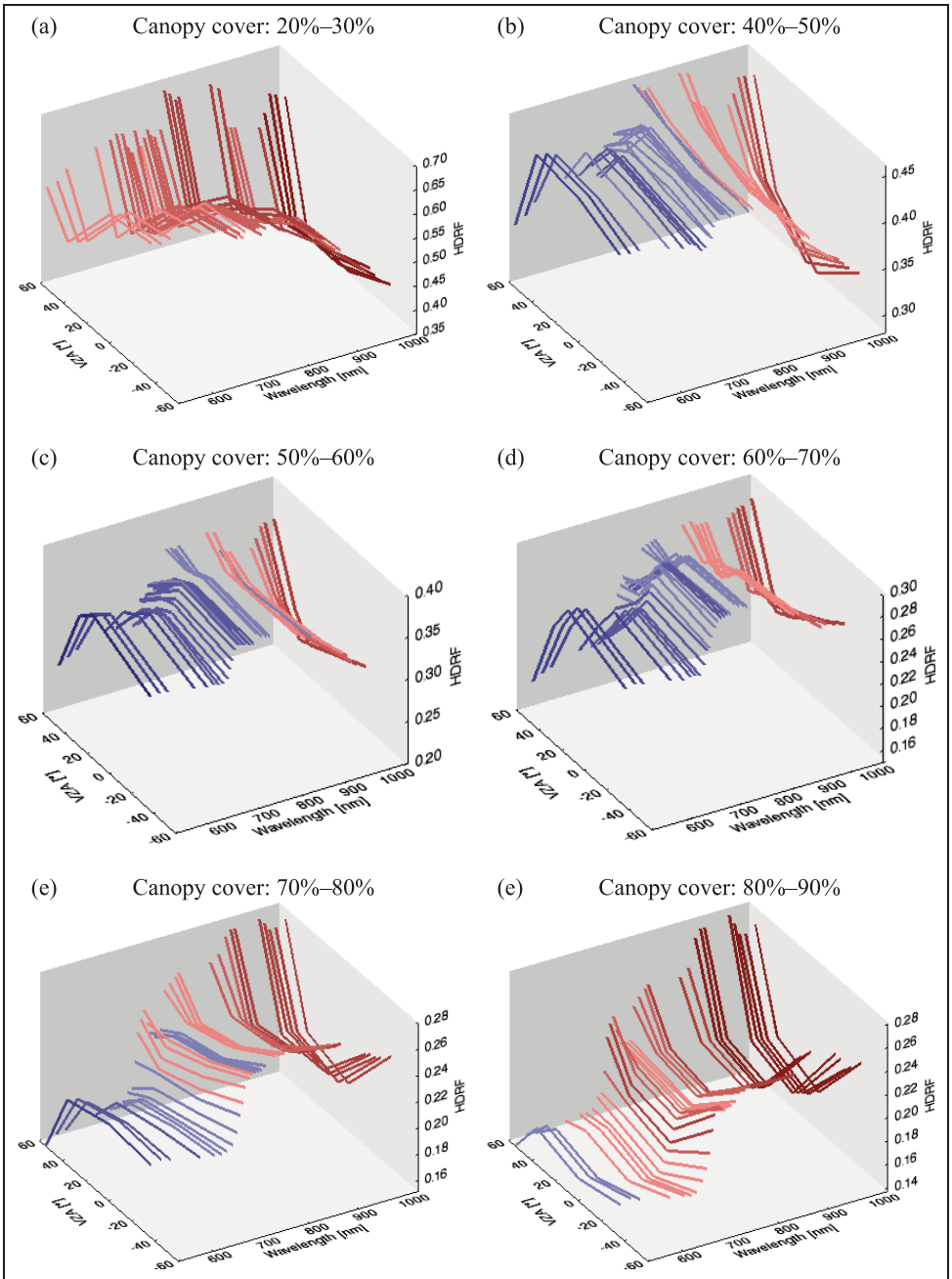

Figure 8. Averaged angular HDRF signatures for 4 canopy cover classes (a, 20%–30%; b, 40%–50%; c, 50%–60%; d, 60%–70%; e, 70%–80%; f, 80%–90%) with a color depending on the Minnaert-*k* value. Negative view zenith angles (VZAs represent the backscattering directions, positive VZAs represent forward scattering directions.

Discussion

Many studies have reported that the use of multiangular data improves assessments of canopy characteristics such as crown cover, tree height, and LAI (Abuelgasim et al., 1996; Bicheron et al., 1997; Braswell et al., 2003; Gobron et al., 2000; Heiskanen, 2006; Liesenberg et al., 2007; Sandmeier and Deering, 1999; Vuolo et al., 2008). They have also amply demonstrated that multiangular data provide additional information; however, all these studies are based on a series of angular data and statistical approaches without explicitly separating the directional information content from the spectral information content. The RPV model is particularly useful for exploring and elucidating the independent contribution of the angular domain. It is a simple model that allows fast decomposition of the scattered radiation into three parameters, of which the Minnaert-*k* parameter relies solely on the curvature of the reflectance anisotropy at a single wavelength. Our work links the RPV's Minnaert-*k* parameter with a subpixel structural heterogeneity variable (canopy cover) at

the scale of the CHRIS subpixel resolution over the full VNIR region including the critical red edge region.

In initial work by Pinty et al. (2002), the use of measurements in the red spectral region was advocated on the grounds that this is where the subpixel reflectance contrast between the vertical, photosynthetically active coniferous trees and the underlying soil cover is maximized. But this assumes summer conditions, where maximum brightness contrast with vegetation is given by a bright bare soil. In a winter landscape, the influence of the underlying bright snow cover is considerably larger (Pinty et al., 2008) (i.e., significant brightness contrast continues throughout the red edge). This greater brightness contrast led to the transition from bell to bowl shapes moving throughout the red edge towards the early NIR. Our work used multiangular CHRIS data to bring the findings of earlier theoretical and broadband studies (e.g., Gobron and Lajas, 2002; Nolin, 2004; Pinty et al., 2002; Widlowski et al., 2001, 2004) into the field of imaging spectrometry. Given the local character of the data set, the results might be subject to uncertainties related to the atmospheric correction procedure, the generation of the base canopy cover map, and the solar zenith angle. Nevertheless, for a set of χ^2-filtered pixels on the valley floor, it has been demonstrated that the bell and bowl shapes of reflectance anisotropy as expressed by the Minnaert-k parameter are bound by physical limitations, by both wavelength and canopy cover. **Figure 7** suggests that the red band is not necessarily always the best band to relate bell and bowl shapes to canopy structure. The figure reveals that for characterizing forest heterogeneity under winter conditions promising results appeared at the end of the red edge (e.g., 735 nm). In this region, blue colour tones ($k > 1.0$, bell shaped) typically indicate the presence of a heterogeneous surface type such as a forest between 40% and 70% cover. Red colour tones ($k < 1.0$, bowl shaped) typically indicate the presence of a structurally homogeneous surface, such as either a sparse tree cover up to 40% or a dense tree cover with a canopy cover over 70%. As well as indicating canopy cover, the Minnaert-k parameter may also act as a vertical profiling proxy within a canopy; high k values are not only related to the occurrence of gap effects, but also to vertical structures within a pixel. For instance, the depth of the bell-shaped curvature for a given canopy cover is additionally controlled by tree height (i.e., tall coniferous trees will result in a more pronounced bell-shaped curvature compared with likewise smaller coniferous trees) because the vertically elongated foliage clumps already obscure the background-leaving radiation at smaller zenith angles. Conversely, low k values characterize pixels in which a vertical profile at the subpixel scale is less marked. This notion of vertical profiling makes the Minnaert-k parameter more distinctive than a canopy cover map; it provides a quantitative indicator of vertical and horizontal heterogeneity at the subpixel scale. Research in this direction was initiated by Widlowski et al. (2001, 2004); using a ray-tracing radiative transfer model they attempted to relate the Minnaert-k parameter to tree density and height. The relationships found were subsequently tested in a real forest stand using a LiDAR dataset (Koetz et al., 2005). Although multiple solutions did occur for a single k value (an example of the well-known, ill-posed problem), canopies with heterogeneity in either the horizontal or vertical dimension were successfully discriminated from homogeneous canopies.

Our results coincide with the work of Kayitakire and Defourny (2004) that reflectance anisotropy in the red edge and early NIR region is critical for canopy characterization. These authors reported that the angular signatures of winter temperate forest types not under snow were significantly different at the red edge and NIR wavelengths of CHRIS. They concluded that canopy structure caused these spectral differences but did not quantify the underlying radiative transfer mechanisms. Progress in this direction was recently made by Rautiainen et al. (2008) who used a radiative transfer model and CHRIS acquisitions during summer. Their modeling results identified the red edge domain as receiving the largest contribution from forest understory, and revealed that the more oblique the view angle, the smaller the direct contribution from the understory. Our work demonstrated some underlying mechanisms (e.g., why a shift in the curvatures of the anisotropic signature occurs).

Variations in angular signatures will be more subtle, however, when the brightness contrast between overstory and background is small (e.g., because of understory). The fraction of sensed shadow cast on the background will then cause the main differences in reflectance anisotropy (Kayitakire and Defourny, 2004). Regardless of the background type, these studies all suggest that the red edge region has strong potential for linking reflectance anisotropy with subpixel surface heterogeneity (e.g., canopy cover, vertical profiling). Further research needs to be done on the anisotropic behaviour of the red edge spectra in relation to biophysical information content. Such research will be of interest for the design of future airborne and spaceborne multiangular sensors.

Despite the good correlations found over flat, forested surfaces, it should be taken into account that several additional factors other than canopy closure are important in shaping the reflectance anisotropy (e.g., the curvature) and, hence, in determining the k parameter. The following potential factors can be identified: (*i*) influence of solar zenith angle (Pinty et al., 2002); (*ii*) remaining contribution from the atmosphere, although largely decoupled, particularly at lower wavelengths; (*iii*) multiple targets contributing to a pixel's angular signature (i.e., background other than snow cover beneath the vegetation canopy (such as rock outcrops or understory) or snow on trees); (*iv*) snow quality affecting anisotropy patterns (Warren et al., 1998); (*v*) influence of horizontal radiation fluxes due to the high spatial resolution of CHRIS (Widlowski et al., 2006); (*vi*) uncertainties related to coregistration of multiangular images; and (*vii*) topographic effects, which, despite being largely decoupled, may still occur (Koetz et al., 2005; Kneubühler et al., 2008). Topographic effects in particular may complicate the robustness of using the Minnaert-k

parameter as a bio-indicator because the presence of topography can lead to enhancement or attenuation of reflectance anisotropy patterns (Schaaf et al., 1994) and therefore affect the relationship between Minnaert-*k* and canopy structure. To overcome the influence of the horizontal radiation fluxes, an alternative may be to coarse-grain the observations from stand to landscape scale (i.e., by using coarser spatial resolution sensors such as MISR data (275 m in red)). At horizontal spatial resolutions of the order of a few hundred metres or more, the net radiation balance of the volume containing the vegetation is largely controlled by the vertical exchanges of radiation with the atmosphere above or the soil below, which dominate the net contributions from horizontal fluxes along the perimeter of that volume (Widlowski et al., 2006). However, at such a low spatial resolution not only variation in canopy cover but also variation in topography and additional land cover types (e.g., rocks, roads, and rivers) govern reflectance anisotropy at the sensor subpixel scale. The subtle variations in anisotropy patterns invoked by vegetation structure tend then to be outperformed by the landscape-scale variations in reflectance anisotropy (e.g., because of riverbeds) (Pinty et al., 2002).

Finally, because the red colour tones in **Figure 7** (bowl-shaped anisotropy patterns; $k < 1.0$) either represent an open snow-covered surface or a dense canopy cover poses another constraint to the interpretation of *k* values for forest mapping applications. This can be easily resolved by combining the Minnaert-*k* map with the spectral dimension of the RPV model (e.g., the amplitude parameter) so that vegetation spectra can be discriminated from the snow spectra. Another option is to combine the Minnaert-*k* map with an independently derived canopy cover map. Spectrodirectional CHRIS data are particularly useful for generating both kinds of maps (e.g., by applying LSU in the spectral domain and Minnaert-*k* retrieval in the directional domain). Merging both products may yield subpixel information beyond what is possible from single-source datasets (Verrelst et al., 2010).

Conclusions

There has been no widespread development of applications making use of both the angular and spectral domains. This paper links anisotropic reflectance signatures of a forested surface as observed from space with forest 3D-heterogeneity at subpixel scale in the spectral domain. We used spectrodirectional CHRIS data to elaborate the exploitation of reflectance anisotropy and more specifically addressed the spectral dependency of the Minnaert-*k* parameter as measured over a coniferous forest. CHRIS images of a coniferous forest acquired during winter were found particularly useful for evaluating the underlying biophysical information embedded in the angular domain. For the set of pixels analyzed, a spectrally driven transition in reflectance anisotropy emerged: from predominantly bell-shaped anisotropy patterns in the visible spectral region toward predominantly bowl-shaped anisotropy patterns in the NIR spectral region. Because of the underlying bright snow cover, the transition from bell to bowl shape for heterogeneous canopies with a canopy cover between 30% and 80% was found somewhere in the red edge region; the exact spectral position of the switch from bell to bowl shape was controlled by canopy cover. The red edge region in particular provided Minnaert-*k* values that were comprehensively related to canopy cover. In this spectral region, medium canopy cover (40%–70%) typically led to bell-shaped anisotropy patterns while canopy covers that were sparse or dense typically led to bowl-shaped reflectance anisotropy patterns. In turn, when the background is less bright than snow cover, the switch from bell to bowl shape is expected to occur earlier in the spectral domain because of reduced brightness contrast. On the application side, these results suggest that a spectral band should be chosen with care when linking reflectance anisotropy to a structural parameter. Further research is required to evaluate the information content of reflectance anisotropy over the full VNIR spectral range under non-snow conditions (e.g., during summer).

Acknowledgements

The work of J. Verrelst was supported through the Dutch SRON GO program (grant EO-080), and the EU Marie Currie FP7-PEOPLE-IEF-2009 grant (grant agreement 252237). CHRIS-PROBA data were acquired under ESA AO proposal 2819 (Swiss National Park). L. Guanter is thanked for assistance with the atmospheric preprocessing. We appreciate the many valuable suggestions of B. Pinty, R. Fernandes, and the anonymous reviewers. J. Burrough advised on the English. V. Laurent is thanked for the translation of the abstract into French.

References

Abuelgasim, A.A., Gopal, S., Irons, J.R., and Strahler, A.H. 1996. Classification of ASAS multiangle and multispectral measurements using artificial neural networks. *Remote Sensing of Environment,* Vol. 57, No. 2, pp. 79–87. doi:10.1016/0034-4257(95)00197-2.

Adams, J.B., Sabol, D.E., Kapos, V., Filho, R.A., Roberts, D.A., Smith, M.O., and Gillespie, A.R. 1995. Classification of multispectral images based on fractions of endmembers: Application to land-cover change in the Brazilian Amazon. *Remote Sensing of Environment,* Vol. 52, No. 2, pp. 137–154. doi:10.1016/0034-4257(94)00098-8.

Asner, G.P., Braswell, B.H., Schimel, D.S., Wessman, C.A. 1998. Ecological research needs from multiangle remote sensing data. *Remote Sensing of Environment,* Vol. 63, No. 2, pp. 155–165. doi:10.1016/S0034-4257(97)00139-9.

Barnsley, M.J., Settle, J.J., Cutter, M.A., Lobb, D.R., and Teston, F. 2004. The PROBA/CHRIS mission: A low-cost smallsat for hyperspectral multiangle observations of the earth surface and atmosphere. *IEEE Transactions on Geoscience and Remote Sensing,* Vol. 42, No. 7, pp. 1512–1520. doi:10.1109/TGRS.2004.827260.

Bicheron, P., Leroy, M., Hautecoeur, O., and Bréon, F.M. 1997. Enhanced discrimination of boreal forest covers with directional reflectances from the airborne polarization and directionality of Earth reflectances

POLDER instrument. *Journal of Geophysical Research D: Atmospheres,* Vol. 102, No. 4, pp. 29 517–29 528.

Borel, C.C., and Gerstl, S.A.W. 1994. Nonlinear spectral mixing models for vegetative and soil surfaces. *Remote Sensing of Environment,* Vol. 47, No. 3, pp. 403–416. doi:10.1016/0034-4257(94)90107-4.

Braswell, B.H., Hagen, S.C., Frolking, S.E., and Salas, W.A. 2003. A multivariable approach for mapping sub-pixel land cover distributions using MISR and MODIS: Application in the Brazilian Amazon region. *Remote Sensing of Environment,* Vol. 87, No. 2–3, pp. 243–256. doi:10.1016/j.rse.2003.06.002.

Canisius, F., and Chen, J.M. 2007. Retrieving forest background reflectance in a boreal region from Multi-angle Imaging SpectroRadiometer MISR data. *Remote Sensing of Environment,* Vol. 107, No. 1–2, pp. 312–321. doi:10.1016/j.rse.2006.07.023.

Chen, X., Vierling, L., Rowell, E., and DeFelice, T. 2004. Using lidar and effective LAI data to evaluate IKONOS and Landsat 7 ETM+ vegetation cover estimates in a ponderosa pine forest. *Remote Sensing of Environment*, Vol. 91, No. 1, pp. 14–26. doi:10.1016/j.rse.2003.11.003.

Chopping, M.J., Rango, A., Havstad, K.M., Schiebe, F.R., Ritchie, J.C., Schmugge, T.J., French, A.N., Su, L., McKee, L., and Davis, M.R. 2003. Canopy attributes of desert grassland and transition communities derived from multiangular airborne imagery. *Remote Sensing of Environment,* Vol. 85, No. 3, pp. 339–354. doi:10.1016/S0034-4257(03)00012-9.

Clevers, J.G.P.W., De Jong, S.M., Epema, G.F., Van der Meer, F.D., Bakker, W.H., Skidmore, A.K., and Scholte, K.H. 2002. Derivation of the red edge index using the MERIS standard band setting. *International Journal of Remote Sensing,* Vol. 23, No. 16, pp. 3169–3184. doi:10.1080/01431160110104647.

Deering, D.W., Eck, T.F., and Banerjee, B. 1999. Characterization of the reflectance anisotropy of three boreal forest canopies in spring-summer. *Remote Sensing of Environment,* Vol. 67, No. 2, pp. 205–222. doi:10.1016/S0034-4257(98)00087-X9

Diner, D.J., Asner, G.P., Davies, R., Knyazikhin, Y., Schaaf, C.B., Muller, J.P., Nolin, A.W., Stroeve, J., and Pinty, B. 1999. New directions in earth observing: Scientific applications of multiangle remote sensing. *Bulletin of the American Meteorological Society,* Vol. 80, No. 11, pp. 2209–2228. doi:10.1175/1520-0477(1999)080<2209:NDIEOS>2.0.CO;2.

Diner, D.J., Beckert, J.C., Reilly, T.H., Bruegge, C.J., Conel, J.E., Kahn, R.A., Martonchik, J.V., Ackerman, T.P., Davies, R., Gerstl, S.A.W., Gordon, H.R., Muller, J.P., Myneni, R.B., Sellers, P.J., Pinty, B., and Verstraete, M.M. 1998. Multi-angle imaging spectroradiometer MISR instrument description and experiment overview. *IEEE Transactions on Geoscience and Remote Sensing,* Vol. 36, No. 4, pp. 1072–1087. doi:10.1109/36.700992.

Diner, D.J., Braswell, B.H., Davies, R., Gobron, N., Hu, J., Jin, Y., Kahn, R.A., Knyazikhin, Y., Loeb, N., Muller, J.P., Nolin, A.W., Pinty, B., Schaaf, C.B., Seiz, G., and Stroeve, J. 2005. The value of multiangle measurements for retrieving structurally and radiatively consistent properties of clouds, aerosols, and surfaces. *Remote Sensing of Environment,* Vol. 97, No. 4, pp. 495–518. doi:10.1016/j.rse.2005.06.006.

Gao, F., Schaaf, C.B., Strahler, A.H., Jin, Y., and Li, X. 2003. Detecting vegetation structure using a kernel-based BRDF model. *Remote Sensing of Environment,* Vol. 86, No. 2, pp. 198–205. doi:10.1016/S0034-4257(03)00100-7.

Gobron, N., and Lajas, D. 2002. A new inversion scheme for the RPV model. *Canadian Journal of Remote Sensing,* Vol. 28, No. 2, pp. 156–167.

Gobron, N., Pinty, B., Verstraete, M.M., Martonchik, J.V., Knyazikhin, Y., and Diner, D.J. 2000. Potential of multiangular spectral measurements to characterize land surfaces: Conceptual approach and exploratory application. *Journal of Geophysical Research D: Atmospheres,* Vol. 105, No. D13, pp. 17 539–17 549.

Guanter, L., Alonso, L., and Moreno, J. 2005. A method for the surface reflectance retrieval from PROBA/CHRIS data over land: Application to ESA SPARC campaigns. *IEEE Transactions on Geoscience and Remote Sensing,* Vol. 43, No. 12, pp. 2908–2917. doi:10.1109/TGRS.2005.857915.

Heiskanen, J. 2006. Tree cover and height estimation in the Fennoscandian tundra-taiga transition zone using multiangular MISR data. *Remote Sensing of Environment,* Vol. 103, No. 1, pp. 97–114. doi:10.1016/j.rse.2006.03.015.

Kayitakire, F., and Defourny, P. 2004. Forest type discrimination using multi-angle hyperspectral data. In *European Space Agency, Special Publication ESA SP* 578, pp. 72–84.

Kneubühler, M., Koetz, B., Huber, S., Schaepman, M.E., and Zimmermann, N.E. 2008. Space-based spectrodirectional measurements for the improved estimation of ecosystem variables. *Canadian Journal of Remote Sensing,* Vol. 34, No. 3, pp. 192–205.

Kneubühler, M., Koetz, B., Richter, R., Schaepman, M., and Itten, K. 2005. Geometric and radiometric pre-processing of CHRIS/PROBA data over mountainous terrain. In *European Space Agency, Special Publication ESA SP* 593 pp. 59–64.

Kötz, B., Schaepman, M., Morsdorf, F., Bowyer, P., Itten, K., and Allgower, B. 2004. Radiative transfer modeling within a heterogeneous canopy for estimation of forest fire fuel properties. *Remote Sensing of Environment,* Vol. 92, No. 3, pp. 332–344. doi:10.1016/j.rse.2004.05.015.

Koetz, B., Kneubülhler, M., Widlowski, J.L., Morsdorf, F., Schaepman, M., and Itten, K. 2005. Assessment of canopy structure and heterogeneity from multi-angular CHRIS-PROBA data. *The 9th International Symposium on Physical Measurements and Signatures in Remote Sensing ISPMSRS*, 17–19 October 2005, Beijing, China, pp. 73–78.

Lavergne, T., Kaminski, T., Pinty, B., Taberner, M., Gobron, N., Verstraete, M.M., Vossbeck, M., Widlowski, J.L., and Giering, R. 2007. Application to MISR land products of an RPV model inversion package using adjoint and Hessian codes. *Remote Sensing of Environment,* Vol. 107, No. 1–2, pp. 362–375. doi:10.1016/j.rse.2006.05.021.

Li, X., and Strahler, A.H. 1992. Geometric-optical bidirectional reflectance modeling of the discrete crown vegetation canopy: Effect of crown shape and mutual shadowing. *IEEE Transactions on Geoscience and Remote Sensing*, Vol. 30, No. 2, pp. 276–292. doi:10.1109/36.134078.

Liesenberg, V., Galvão, L.S., and Ponzoni, F.J. 2007. Variations in reflectance with seasonality and viewing geometry: Implications for classification of Brazilian savanna physiognomies with MISR/Terra data. *Remote Sensing of Environment,* Vol. 107, No. 1–2, pp. 276–286. doi:10.1016/j.rse.2006.03.018.

Minnaert, M. 1941. The reciprocity principle in lunar photometry. *Astrophysical Journal,* Vol. 93, pp. 403–410. doi:10.1086/144279.

Morsdorf, F., Meier, E., Kötz, B., Itten, K.I., Dobbertin, M., and Allgöwer, B. 2004. LIDAR-based geometric reconstruction of boreal type forest stands at single tree level for forest and wildland fire management. *Remote Sensing of Environment,* Vol. 92, No. 3, pp. 353–362. doi:10.1016/j.rse.2004.05.013.

Nolin, A.W. 2004. Towards retrieval of forest cover density over snow from the Multi-angle Imaging SpectroRadiometer MISR. *Hydrological Processes,* Vol. 18, No. 18, pp. 3623–3636. doi:10.1002/hyp.5803.

Painter, T.H., and Dozier, J. 2004. The effect of anisotropic reflectance on imaging spectroscopy of snow properties. *Remote Sensing of Environment,* Vol. 89, No. 4, pp. 409–422. doi:10.1016/j.rse.2003.09.007.

Pinty, B., Gobron, N., Widlowski, J.L., Lavergne, T., and Verstraete, M.M. 2004. Synergy between 1-D and 3-D radiation transfer models to retrieve vegetation canopy properties from remote sensing data. *Journal of Geophysical Research D: Atmospheres,* Vol. 109, No. D21205, pp. 1–16.

Pinty, B., Lavergne, T., Kaminski, T., Aussedat, O., Giering, R., Gobron, N., Taberner, M., Verstraete, M.M., Voβbeck, M., and Widlowski, J.L. 2008. Partitioning the solar radiant fluxes in forest canopies in the presence of snow. *Journal of Geophysical Research D: Atmospheres,* Vol. 113, No. 4, pp D04104. doi:10.1029/2007JD009096.

Pinty, B., Widlowski, J.L., Gobron, N., Verstraete, M.M., and Diner, D.J. 2002. Uniqueness of multiangular measurements - Part I: An indicator of subpixel surface heterogeneity from MISR. *IEEE Transactions on Geoscience and Remote Sensing,* Vol. 40, No. 7, pp. 1560–1573. doi:10.1109/TGRS.2002.801148.

Rahman, H., Verstraete, M.M., and Pinty, B. 1993. Coupled Surface-Atmosphere Reflectance Csar Model .2. Semi-empirical surface model usable with NOAA Advanced Very High Resolution Radiometer data. *Journal of Geophysical Research-Atmospheres,* Vol. 98, No. D11, pp. 20 791–20 801.

Rautiainen, M., Lang, M., Möttus, M., Kuusk, A., Nilson, T., Kuusk, J., and Lükk, T. 2008. Multi-angular reflectance properties of a hemiboreal forest: An analysis using CHRIS PROBA data. *Remote Sensing of Environment,* Vol. 112, No. 5, pp. 2627–2642.

Sabol Jr, D.E., Gillespie, A.R., Adams, J.B., Smith, M.O., and Tucker, C.J. 2002. Structural stage in Pacific Northwest forests estimated using simple mixing models of multispectral images. *Remote Sensing of Environment,* Vol. 80, No. 1, pp. 1–16. doi:10.1016/S0034-4257(01)00245-0.

Salisbury, J.W., D'Aria, D.M., and Wald, A. 1994. Measurements of thermal infrared spectral reflectance of frost, snow, and ice. *Journal of Geophysical Research,* Vol. 99, No. B12, pp. 24 235–24 240.

Sandmeier, S., and Deering, D.W. 1999. Structure analysis and classification of boreal forests using airborne hyperspectral BRDF data from ASAS. *Remote Sensing of Environment,* Vol. 69, No. 3, pp. 281–29. doi:10.1016/S0034-4257(99)00032-25.

Schaaf, C.B., Li, X., and Strahler, A.H. 1994. Topographic effects on bidirectional and hemispherical reflectances calculated with a geometric-optical canopy model. *IEEE Transactions on Geoscience and Remote Sensing,* Vol. 32, No. 6, pp. 1186–1193. doi:10.1109/36.338367.

Schaepman, M.E., Kötz, B., Schaepman-Strub, G., and Itten, K.I. 2005. Spectrodirectional remote sensing for the improved estimation of biophysical and -chemical variables: Two case studies. *International Journal of Applied Earth Observation and Geoinformation,* Vol. 63, No. 4, pp. 271–282. doi:10.1016/j.jag.2004.10.012.

Schaepman-Strub, G., Schaepman, M.E., Painter, T.H., Dangel, S., and Martonchik, J.V. 2006. Reflectance quantities in optical remote sensing-definitions and case studies. *Remote Sensing of Environment,* Vol. 103, No. 1, pp. 27–42. doi:10.1016/j.rse.2006.03.002.

Sedano, F., Lavergne, T., Ibañez, L.M., and Gong, P. 2008. A neural network-based scheme coupled with the RPV model inversion package. *Remote Sensing of Environment,* Vol. 112, No. 7, pp. 3271–3283. doi:10.1016/j.rse.2008.04.003.

Settle, J.J., and Drake, N.A. 1993. Linear mixing and the estimation of ground cover proportions. *International Journal of Remote Sensing,* Vol. 14, No. 6, pp. 1159–1177. doi:10.1080/01431169308904402.

Smolander, S., and Stenberg, P. 2003. A method to account for shoot scale clumping in coniferous canopy reflectance models. *Remote Sensing of Environment,* Vol. 88, No. 4, pp. 363–373. doi:10.1016/j.rse.2003.06.003.

Toutin, T. 2004. Geometric processing of remote sensing images: Models, algorithms and methods. *International Journal of Remote Sensing,* Vol. 25, No. 10, pp. 1893–1924. doi:10.1080/0143116031000101611.

Verhoef, W. 1984. Light scattering by leaf layers with application to canopy reflectance modeling: The SAIL model. *Remote Sensing of Environment,* Vol. 16, No. 2, pp. 125–141. doi:10.1016/0034-4257(84)90057-9.

Verrelst, J., Clevers, J.G.P.W., Schaepman,M.E. 2010. Merging Minnaert-k parameter with spectral unmixing to map forest heterogeneity with CHRIS-PROBA data. *IEEE Transactions on Geoscience and Remote Sensing,* Vol. 48, No. 11, pp. 4014–4022.

Verrelst, J., Schaepman, M.E., Koetz, B., and Kneubühler, M. 2008. Angular sensitivity analysis of vegetation indices derived from CHRIS/PROBA data. *Remote Sensing of Environment,* Vol. 112, No. 5, pp. 2341–2353.

Verstraete, M.M., Pinty, B., and Dickinson, R.E. 1990. A physical model of the bidirectional reflectance of vegetation canopies: 1. Theory. *Journal of Geophysical Research,* Vol. 95, No. 11, pp. 755–11765.

Vikhamar, D., and Solberg, R. 2003. Subpixel mapping of snow cover in forests by optical remote sensing. *Remote Sensing of Environment,* Vol. 84, No. 1, pp. 69–82. doi:10.1016/S0034-4257(02)00098-6.

Vuolo, F., Dini, L., and D'Urso, G. 2008. Retrieval of Leaf Area Index from CHRIS/PROBA data: an analysis of the directional and spectral information content. *International Journal of Remote Sensing,* Vol. 29, pp. 5063–5072. doi:10.1080/01431160802036490.

Warren, S.G., Brandt, R.E., and Hinton, P.O. 1998. Effect of surface roughness on bidirectional reflectance of Antarctic snow. *Journal of Geophysical Research E: Planets,* Vol. 103, No. E11, pp. 25 789–25 807.

Widlowski, J.L., Pinty, B., Gobron, N., Verstraete, M.M., and Davis, A.B. 2001. Characterization of surface heterogeneity detected at the MISR/TERRA subpixel scale. *Geophysical Research Letters,* Vol. 28, No. 24, pp. 4639–4642. doi:10.1029/2001GL013490.

Widlowski, J.L., Pinty, B., Gobron, N., Verstraete, M.M., Diner, D.J., and Davis, A.B. 2004. Canopy structure parameters derived from multi-angular remote sensing data for terrestrial carbon studies. *Climatic Change,* Vol. 67, No. 2–3, pp. 403–415. doi:10.1007/s10584-004-3566-3.

Widlowski, J.L., Pinty, B., Lavergne, T., Verstraete, M.M., and Gobron, N. 2006. Horizontal radiation transport in 3-D forest canopies at multiple spatial resolutions: Simulated impact on canopy absorption. *Remote Sensing of Environment*, Vol. 103, No. 4, pp. 379–397. doi:10.1016/j.rse.2006.03.014.

Zurita-Milla, R., Clevers, J.G.P.W., Schaepman, M.E., and Kneubühler, M. 2007. Effects of MERIS L1b radiometric calibration on regional land cover mapping and land products. *International Journal of Remote Sensing,* Vol. 28, No. 3–4, pp. 653–673. doi:10.1080/01431160600821069.